Development of a Lunar Lander Modeling and Simulation Capability

Eugina Mendez Ramos *, Bradford Robertson †, Manuel J. Diaz ‡, and Dimitri Mavris §
Georgia Institute of Technology, Atlanta, GA, 30332

The development and validation of a capability to perform quantitative, physics-based analysis of alternatives of conceptual unmanned, reusable lunar cargo lander architectures is discussed. The lander is conceptualized as a suite of disciplines that need to be sized, synthesized, and optimized for a mission. As such, models of these disciplines were developed and integrated in a recently-developed multi-disciplinary analysis and optimization framework for space systems. The development of the disciplines, as well as how they are integrated into the framework, is discussed. Additionally, validation studies were performed against the Descent Module of the Altair lunar lander. Finally, an example problem for an uncrewed, reusable lander is presented.

Nomenclature

AoA	=	Analysis of Alternatives
d	=	diameter (m)
DYREQT	=	DYnamic Rocket EQuation Tool
F	=	Thrust (N)
FPR	=	Flight Performance Reserve
F / W	=	Thrust-to-Weight Ratio
I_{sp}	=	Specific Impulse (s)
LAD	=	Liquid Acquisition Device
LH_2	=	Liquid Hydrogen
LOX	=	Liquid Oxygen
m	=	Mass (kg)
$\dot{m}$	=	Mass Flow Rate (kg/s)
MGA	=	Mass Growth Allowance
MDAO	=	Multidisciplinary Design, Analysis, and Optimization
MLI	=	Multi-Layer Insulation
MMH	=	Monomethyl Hydrazine
MPS	=	Main Propulsion System
MR	=	Manger's Reserve
M&S	=	Modeling and Simulation
NTO	=	Nitrogen Tetroxide
P	=	Power (W)
p	=	Payload (kg)
$\dot{Q}$	=	Heat Rate (W)
RCS	=	Reaction Control System
T	=	Temperature (K)

*Senior Graduate Researcher,Aerospace Systems Design Laboratory, School of Aerospace Engineering, AIAA Student Member
†Research Engineer II, Aerospace Systems Design Laboratory, School of Aerospace Engineering, AIAA Member
‡Senior Graduate Researcher,Aerospace Systems Design Laboratory, School of Aerospace Engineering, AIAA Student Member
§S.P. Langley Distinguished Regents Professor and ASDL Director, Aerospace Systems Design Laboratory, School of Aerospace Engineering, AIAA Fellow.

I. Introduction

The United States of America's National Space Policy has a goal of returning humans to the moon in the 2020s. The proposed plan has initial sortie missions in the mid-2020s followed by the creation of the first lunar base– Artemis Base Camp [1]. A key enabler for the establishment and sustainment of a lunar base is a cargo lunar lander. Furthermore, future cargo landers will have to work within the existing lunar architecture as defined by the Human Landing System and Gateway.

In realizing the goal of access to and from the lunar surface, an Analysis of Alternatives (AoA) study is necessary to evaluate, analyze, and trade the potentially many legitimate courses of action before down-selecting to one or a few attractive options. In order to conduct an AoA in an efficient fashion during the early stages of design, a process that utilizes a rapid, flexible, quantitative Modeling and Simulation (M&S) environment is required. The M&S environment should enable analysts to evaluate alternatives by sizing the disciplines – e.g. avionics, structures, power, tanks, engines, thermal, etc., i.e. it must employ Multidisciplinary Design, Analysis, and Optimization (MDAO) – that must be synthesized to define a lunar lander and mission concept. Quantitative evaluation during conceptual design is realized via the use of engineering tools, which may be physics-based or historical-based. Rapid evaluation consists of utilizing automated engineering tools that are also inexpensive to run. However, developing such an MDAO environment is traditionally a labor-intensive, architecture-specific process, and therefore still has many barriers to entry that prevent its use from being widely adopted for pre-conceptual and conceptual design studies. As a result, the number of architectures considered in a typical AoA is directly proportional to the degree of analyst-based resources allocated. In the case of lunar landers and space systems in general, this issue is further exacerbated, as vehicle and mission architectures, technologies, and other considerations need to be traded, leading to a prohibitive number of cases to evaluate, or conversely, a limited number of architectures to consider; which architectures are considered are usually selected by the analysts. If the successful acquisition and operation of a lunar lander as part of a larger ecosystem is desired, then the capability to perform quantitative AoA during pre-conceptual and conceptual design is necessary to identify and select the best alternatives, therefore, enabling informed decision-making.

In this paper, we briefly present a recently-developed M&S framework, the Dynamic Rocket Equation Tool (DYREQT)[2, 3], that addresses this critical need by rapidly sizing, synthesizing, and optimizing a given space system by adopting a model-based, object-oriented approach. Because there are numerous engineering tools for sizing space systems, one of the key features DYREQT incorporates is that it allows analysts to integrate their own codes. To demonstrate the capability for rapid AoA provided by the DYREQT framework, the capability is applied here to a reusable lunar lander concept. The lander can be conceptualized as a collection of disciplines, or subsystems; these disciplines are represented as modules and are integrated into the DYREQT framework. The development of the subsystem models is discussed in Section III. In Section IV, the M&S capability is validated against the Descent Module of the Altair DAC-3. Finally, M&S environment is applied to a reusable cargo lunar lander concept in Section V.

II. Overview of DYREQT

The design of any engineered system is widely understood to be a decision-making process; the case of pre-conceptual and conceptual design of space systems is no exception. The process of designing space systems is generally characterized as a tightly-coupled problem in which decisions cannot be reduced to high-level metrics, e.g. propellant mass fractions, a priori. This leads to the requirement that space systems must be modeled at the subsystem level.[4] Therefore, in order to assess the impact of each decision, the subsystems need to be synthesized to define a vehicle architecture and sized to perform a given mission. Additionally, the process for the closure of space systems is non-linear[5], making this a difficult, tightly-coupled MDAO problem that further exacerbates the problem. However, one of the major impediments to performing physics-based MDAO during pre-conceptual and conceptual design is that it often requires considerable resources early on to set up the associated MDAO environment with the required contributing analyses, or disciplines. As a result, organizations tend to adopt manual, ad-hoc design processes where few candidates are evaluated and traded.[6] In order to overcome these barriers, DYREQT was developed and will be briefly introduced in this section.

The key tenets of DYREQT are that it applies model-based engineering and object-oriented philosophies to space systems, utilizes modern DYREQT techniques, and allows users to "bring your own codes."[2] The object-oriented philosophy allows users to define and specify almost any arbitrary space system architecture via an ontology. Within this ontology, a space systems architecture is comprised of a unique vehicle and mission definition. The vehicle is defined as a unique sequence of elements, e.g. payloads and stages; the mission is comprised of a sequence of events. The vehicle's elements are further comprised of subelements, which represent subsystems, e.g. a stage (an 'element' in DYREQT jargon) is comprised of tanks, engines, etc. ('subelements' in DYREQT jargon); if the user is not interested

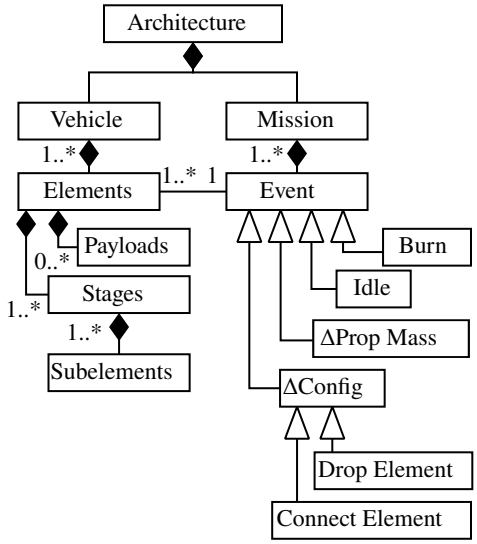

Fig. 1 Ontology used by DYREQT to model space system architectures

in modeling a constituent element, it is referred to as a 'payload.' Similarly, a mission is defined as a unique sequence of events. Each event can be one of four types: a burn, a passage of time, an inert mass change, or a propellant mass change; each affects one or more vehicle elements, forming a mission-to-vehicle mapping. This ontology is shown in Figure 1. This ontology also serves as the basis for how the individual subelements will be sized: DYREQT enables users to size each subelement and event through engineering codes, thus employing an approach that allows the usage of existing codes with little to no modifications via a "wrapper." Due to the flexibility of the Python programming language, the individual subelements themselves can evaluate pure Python or external, e.g. FORTRAN, C, Excel, etc., engineering analyses. Additionally, DYREQT reformulates the traditional space systems sizing and synthesis problem such that it is amenable to standard MDAO techniques.[2] As such, DYREQT leverages OpenMDAO[7, 8] and its state-of-the-art solvers; each subelement is an OpenMDAO-based 'wrapper' that handles its inputs, execution of the code, and its outputs. The DYREQT framework instantiates an OpenMDAO-based discipline for every mission event, vehicle subelement, and performs many intermediate calculations necessary to model space systems. With the instantiated disciplines, the MDAO environment is assembled at run time and solved. OpenMDAO handles the finite differencing, fixed-point iterations, etc., in order for each solution to be multi-disciplinary feasible. The user has the option of leveraging OpenMDAO's optimization drivers, performing Design of Experiments, or simply evaluating a single candidate solution. In the case of the lunar lander concept, several subsystems need to be synthesized and sized in order to model a lander system. As such, a suite of modules was developed to model all necessary subsystems and subsequently integrated within DYREQT. The development of these subsystem modules is discussed in Section III.

III. Development of Modules

Six subsystem models were developed in order to represent a lunar lander with the proper level of detail to allow for an AoA. These models include the avionics, power, structures, engines, tanks, and thermal control subsystems. The subsystem models work collectively with DYREQT to size mass, power, and thermal loads. Details regarding the sizing routine for each subsystem is provided in the sections that follow.

A. Avionics

The Avionics model sizes hardware associated with sensing, actuating, and communication based on the mass and power data of flight-certified, commercially available hardware [9]. The model allows the selection of set of actuators, sensors, and communications packages to utilize on the vehicle. Available options for actuators include reaction wheels, control moment gyros, and magnetic torquers; sensor options include gyros, sun and star (fixed or scanner) sensors, horizon sensors, and a magnetometer.

The subsystem mass is the sum of the masses of the sensors, actuators, communications package, and any additional

devices:

$$m_i = \frac{m_{sensors} + m_{actuators} + m_{coms} + m_{other}}{f_{cable}} \tag{1}$$

The actuators scale with vehicle mass, the sensors scale via an accuracy factor, and the communications package scales with the operational distance from the Earth. Additional devices not listed above are accepted; in this case relationship between the mass (m_{other}) and power requirement (P_{other}) for the device must be specified. Finally, the term in the denominator of Equation 1 accounts for wireless sensor technologies by applying a factor, f_{cable}, for cabling reduction to the overall subsystem mass.

The total power requirement for the subsystem is the sum of the power required by the individual components. The heat load generated is estimated to be 90% of the total subsystem power:

$$P_{req} = P_{sensors} + P_{actuators} + P_{coms} + P_{other} \tag{2}$$

$$\dot{Q}_{total} = 0.9 P_{req} \tag{3}$$

B. Power

The mass of the power subsystem is based on three primary components - the generator, power storage, and regulation/distribution:

$$m_{inert} = m_{generator} + m_{storage} + m_{distribution} \tag{4}$$

The model receives the power requirements from each of the subsystem models (where applicable) as an input and sizes the primary generator to satisfy the total power requirement for the lander. Power in the form of storage is sized to provide power for the lander during operations in eclipse, plus an additional margin if desired. Primary power generator options include photovoltaic solar arrays and alkaline fuel cells. Solar array mass is calculated using level-zero physics-based equations in Wertz [9]; fuel cells are sized based on relationships provided by Komar et al.[6]. Energy storage is provided by rechargeable lithium ion batteries, with the battery mass calculated from the capacity, specific energy, and number of batteries required. The mass of the regulation and distribution are lumped together, and is approximately 20% of the generator and storage mass[9].

The total thermal load produced by the subsystem is sum of the contributions from the generator and the batteries:

$$\dot{Q}_{total} = \dot{Q}_{generator} + \dot{Q}_{storage} \tag{5}$$

If solar arrays are used, the contribution to the total heat load from the generator is zero – batteries become the sole contributor to the total heat load.

C. Structures

In an attempt to estimate the structure mass, data on a variety of space systems – landers, ascent/descent modules, satellites, spacecraft, etc. – was collected [9–15]. The data was categorized by system type, and a least squares regression applied to each to determine the average percentage of the structure-to-vehicle dry mass. Table 1 lists the systems considered, along with the average corresponding structure percentage of that category, the coefficient of determination, and the number of data points used in the regression, represented as δ, R^2, and N, respectively. The subsystem mass is estimated using Equation 6, where X denotes the (fractional) portion of the vehicle dry mass that is dedicated to the structure:

$$m_i = X m_{vehicle} \tag{6}$$

D. Engines

The engines subsystem model sizes bipropellant liquid engines based on the scaling equations presented in Humble[16]. The subsystem mass consists of the engine, propellant management hardware associated with the physical engine such as valves, regulators, filters, transducers, and miscellaneous components such as plumbing, brackets, and insulation:

Table 1 Data for Obtaining Structures Percentage

System	δ	R^2	N
Cruise Stage	26.3	0.998	3
General Satellite	28.8	0.922	81
General Spacecraft	27.4	0.935	104
Lander	22.0	0.954	5
Reentry Module	34.3	0.979	4
Total Vehicle	28.0	0.966	7

$$m_i = m_{engines} + m_{propmgt} + m_{misc} \tag{7}$$

Propellant management hardware is assumed to be 10% of the engine mass; miscellaneous hardware is assumed to be 15% of the mass of engine(s) and the propellant management hardware. Engine mass scales with thrust via the relationships in Equations 8 and 9. The top relation in Equation 9 is representative of the thrust class of in-space bi-propellant engines, whereas the bottom relation is representative of the thrust class of engines used on the first stage of launch vehicles.[16]

$$m_{engines} = n_{engines} m_{eng} \tag{8}$$

$$m_{eng} = \begin{cases} \frac{T/g_0}{6.098\times10^{-4}T+13.44}, & F < 50 \text{ kN} \\ \frac{T/g_0}{25.2\log(T)-80.7}, & F \geq 50 \text{ kN} \end{cases} \tag{9}$$

E. Tanks

Propellant and pressurant tank masses for the main propulsion system (MPS) and the reaction control system (RCS) are estimated based on information such as propellant mass, propellant types, propellant properties, pressurant type, number of tanks, and tank material properties. The subsystem mass consists of the mass of the tank(s), liquid acquisition devices (LAD), miscellaneous hardware, and additional pressurant and propellant masses:

$$m_i = \sum_{i=1}^{n_{tanks}} m_{tank_i} + m_{lad_i} + m_{misc_i} + m_{pres_i} + m_{trap_i} \tag{10}$$

The LAD is estimated to be 53.7% of the tank mass[17]. Miscellaneous hardware such as plumbing, brackets and insulation is estimated to be 15% of the tank mass. The pressurant mass is sized to fully expel the propellant from the tank, whereas trapped propellant is assumed to be 1% of the total useable propellant. The tank mass includes the bare mass of the tank itself, plus additional hardware such as weld lands, inlet/outlet flanges, structural attach points, and a seperator device, when required:

$$m_{tank} = m_{bare} + m_{weld} + m_{IO} + m_{sa} + m_{sep} \tag{11}$$

The bare tank mass is estimated using level-zero physics-based equations from Chapman for calculating propellant volumes and subsequent wall thickness of the tank[18]. Tank shape is determined by the length-to-diameter (L/D) ratio, where the size of the tank is determined by the number of tanks and the total propellant volume to disperse among those tanks. Tank geometry can be spherical, or cylindrical with hemispherical end caps.

F. Thermal Control

Sizing of the vehicle thermal control systems is sectioned into three parts. Sizing of the passive system occurs first, followed by the active system, and concludes with sizing of the heat rejection system. Passive and active sizing routines size thermal control components for tanks containing liquid hydrogen (LH_2), liquid oxygen (LOX), and liquid methane (LCH_4) via NASA's Cryogen Storage Integrated Model (CryoSIM), a cryogenic fluid management (CFM) system sizing tool for use in conceptual and preliminary design of in-space cryogenic storage systems [17]. Once the sizing routine

has stepped through each of the passive, active, and heat rejection systems, the total mass and power requirement for the thermal control subsystem are determined using the following equations:

$$m_i = m_{passive} + m_{active} + m_{heat\ rejection} \tag{12}$$

$$P_{total} = P_{passive} + P_{active} + P_{heat\ rejection} \tag{13}$$

The methods for estimating the mass and power requirements of the passive and active systems using CryoSIM are described in Sections III.F.1 and III.F.2, respectively. Heat rejection is discussed in Section III.F.3.

1. Passive CFM

Passive CFM systems consist of variable density multi-layer insulation (MLI), spray on foam insulation (SOFI), and a mass gauging device. The MLI consists of three sections - an inner, middle, and outer segment, each with a corresponding density. The model takes in the total number of layers as an input, determines how to distribute the layers among each of the inner, middle, and outer segments, then subsequently calculates the mass of the MLI based on the number of layers in the segment and the density of that segment. The mass of the SOFI is determined using input values for density and thickness. The mass of the mass gauging device scales with the longest dimension of the tank. The only component with a power requirement is the mass gauge, which is also scales with the longest dimension of the tank.

$$m_{passive} = m_{mli} + m_{SOFI} + m_{gauge} \tag{14}$$

$$P_{passive} = P_{gauging} = f(\max(d_{tank}, l_{tank})) \tag{15}$$

In addition to the subsystem mass and power, the model also outputs the propellant boil-off rate. Based on the mission type – in-space or planetary – and information on the spacecraft thermal environment, the model estimates the effective environmental temperature, or hotside temperature (T_h), on the propellant tank. From T_h and the propellant temperature T_c, the total heat load on the tank can be determined. Contributions include the heat that penetrates the MLI and enters the tank and the heat due to thermal conductance of the warmer tank support structure and penetrations:

$$\dot{Q}_{total} = \dot{Q}_{mli} + \dot{Q}_{struct} + \dot{Q}_{penet} \tag{16}$$

where,

$$\dot{Q}_{mli} = f(T_h, T_c, n_{layers}, \epsilon_{mli}) \tag{17}$$

$$\dot{Q}_{struct}, \dot{Q}_{penet} = f(T_h, T_{int}, \kappa) \tag{18}$$

The heat through the MLI is calculated using the Modified Lockheed Equation in Hastings [19]. The temperature of the support structure and penetrations (T_{int}) is dependent upon the storage temperatures of the propellants being used. It is assumed that the structure and penetration temperature for the propellant with the colder storage temperature is at some intermediate temperature ($T_{low} < T_{int} < T_{high}$), while the structure and penetration temperature of the propellant with the higher storage temperature is at the same temperature ($T_{int} = T_{high}$):

$$T_{int} = \begin{cases} \frac{2}{3}(T_{high} - T_{low}) + T_{low}, & \text{colder liquid} \\ T_{high}, & \text{warmer liquid} \end{cases} \tag{19}$$

The structure and penetration temperature impacts the thermal conductivity, and thus, the heat entering the tank. The assumption imposes an aspect of sensitivity and susceptibility of the LH_2 tank to the surrounding environment, with a much less pronounced effect for LOX/LCH_4 where the storage temperatures are similar. Once all the thermal contributions on the tank have been defined, the boil-off rate ($\dot{m}_{propellant}$) can be determined from the heat entering the tank and the enthalpy of vaporization (h_{vap}) of the propellant:

$$\dot{m}_{propellant} = \frac{\dot{Q}_{total}}{h_{vap}} \tag{20}$$

2. Active CFM

Active cooling of cryogenic propellants in CryoSIM is accomplished via Broad Area Cooling (BAC), which utilizes cryocoolers and a pressurized working fluid circulation system to intercept heat loads on the propellant tank. Heat is intercepted by a gas-cooled radiation shield (BAC shield) embedded within the MLI of the LH_2 tank, or by cooling tubes attached to the external tank wall of LOX and LCH_4 tanks[17, 20]. CryoSIM supports the analysis of the following active CFM configurations and propellant combinations:

- Zero Boil-Off (ZBO) of LOX/LCH_4
- ZBO of LOX/LH_2
- Reduced Boil-Off (RBO) of LOX/LH_2

ZBO LOX/LCH_4 and RBO LOX/LH_2 systems utilize 90 K cryocoolers of 20 W cooling capacity, while the ZBO LOX/LH_2 system utilizes 90 K and 20 K cryocoolers of 20 W cooling capacity on the LOX and LH_2 tanks, respectively. ZBO options result in crycoolers that are sized to completely remove the heat entering the tank ($\dot{Q}_{total}$), resulting in ZBO for both fuel and oxidizer tank(s). The RBO option, while it doesn't completely remove boil-off, provides a substantial reduction in the LH_2 tank when compared to boil-off rates obtained through passive means alone [21].

The active CFM system mass consists of the masses of the cryocoolers and BAC shields. Masses are based on scaling equations for the cryocooler and shield. The cryocooler mass includes associated hardware such as the recuperator, compressor, accumulators and tubing. The shield mass includes components such as tubing, support structure, fittings, inlet/outlet flanges, manifolds, etc. The power requirement for the active CFM system consists of the power required to run the cryocooler and circulator and is based on scaling equations provided by CryoSIM.

$$m_{active} = m_{cc} + m_{bac} \tag{21}$$

$$P_{active} = P_{cc} + P_{circ} \tag{22}$$

$$\dot{Q}_{total} = \sum_{i=1}^{n_{cc}} \dot{Q}_{lift_i} \tag{23}$$

The total heat load, while an output for the active CFM sizing routine, becomes an input for the next and final step in the sizing process of the thermal control subsystem - the sizing of the vehicle heat rejection system.

3. Heat Rejection

Heat rejection for the lander is accomplished with a passive thermal radiator. The excess heat rejected by the radiator to the environment is the culmination of the heat loads from each of the subsystems, including the heat intercepted by the cryocoolers. The radiator is sized using level-zero physics-based equations and values provided in Wiley[22]. High-efficiency radiators are available as a technology option, and the radiator density is available as an input.

$$m_{rad} = A_{rad}\rho_{rad} \tag{24}$$

$$A_{rad} = \frac{\sum \dot{Q}_{total}}{\sigma \epsilon_{rad} \eta_{rad} (T_{rad}^4 - T_{space}^4)} \tag{25}$$

The radiator surface temperature is assumed to be 250K, and rejects heat away from the spacecraft and to the external space environment, which is approximately 2.7 K. The radiator density is assumed to be 5 kg/m^3, with a nominal efficiency of 0.85.

IV. Validation of the M&S Environment

In order to validate the newly developed capability, the Altair descent module (DM) was identified as a suitable vehicle to benchmark against. Inputs and assumptions that were used in the mission and vehicle definitions are discussed in Sections IV.A and IV.B, respectively. The resulting high-level dry mass breakdown and total vehicle mass obtained from the M&S environment are presented in Section IV.C.

A. Altair DM Mission

The Altair DM is sized based on information gathered from published Constellation program missions.[23] The Concept of Operations (CONOPS) for a standard lunar sortie mission is shown in Figure 2. The Altair is launched aboard an Ares V heavy lift launch vehicle and is followed by the Orion spacecraft and crew a few days later aboard an Ares I. While in LEO, Orion and crew detach from Ares I and dock with Altair on Ares V. The Ares V Earth departure stage then places the Altair and Orion “stack" into trans-lunar injection (TLI). The Altair DM is then responsible for all propulsive maneuvers that follow. After TLI, the DM performs a lunar orbit insertion (LOI) maneuver. After arriving in low lunar orbit (LLO), the crew transfer from Orion into the Altair ascent module, and Orion detaches from the stack. The DM performs the braking burn and final approach maneuvers until touchdown on the lunar surface. The ΔV budget for this mission and other key mission events is detailed in Table 2. Table 3 lists the payloads carried by the DM over the course of the mission. As stated previously, the Orion and crew are carried by the DM during LOI and in LLO, at which point Orion undocks with Altair (minus astronauts). The DM then carries the ascent module, airlock, payload, and astronauts to the lunar surface.

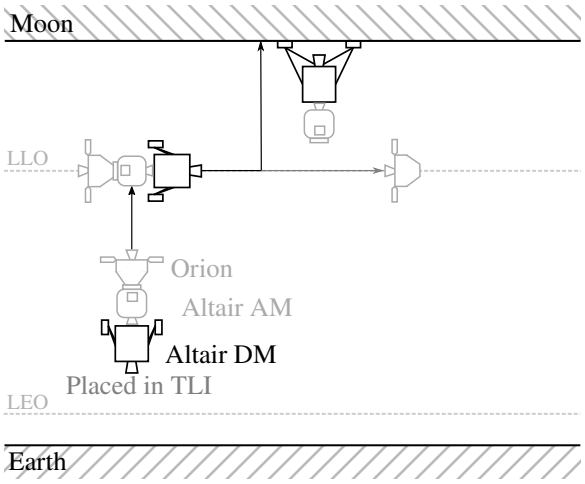

Fig. 2 Altair CONOPS

B. Altiar DM Vehicle

Vehicle information for the Altair DM was gathered from Polsgrove[25], Stephan[26], and LDAC-3[27]. Where necessary, assumptions were used in order to satisfy any remaining gaps in the vehicle definition. Sections IV.B.1 through IV.B.6 present the inputs that were used to size the DM subsystems.

1. Avionics

The avionics suite consists of three reaction wheels and six control moment gyros. The sensing equipment suite on board includes three gyros, three star scanners, a horizon sensor, a magnetometer, and terrain and hazard navigation. Lastly, the DM carries deep space communication antennae and related equipment.

2. Power

Primary power is provided by alkaline fuel cells; supplemental power storage is provided by rechargeable Li-Ion batteries. The fuel cell stack is sized to satisfy the 4.5 kW continuous power requirement for lunar surface operations[25], with an assumed transmission efficiency of 90% and a power density of 60 W/kg. While a single fuel cell stack is sufficient to accommodate the power requirement, two additional fuel cells are included for redundancy. The batteries are sized to provide the additional 1.5 kW requirement during transition from LLO to the lunar surface[25], and are assumed to have a maximum depth of discharge of 50% and a specific storage capacity of 125 W-h/kg. As with the fuel cells, an additional two batteries are included for redundancy.

Table 2 Altair Sortie Mission [23]

Event	Propulsion System	Metric
LEO Loiter		4 days
TCM Burns	RCS	25.4 m/s
Lunar Transit		4 days
LOI Settling Burn	RCS	0.6 m/s
LOI-1	MPS	326 m/s
LOI-2	MPS	59 m/s
LOI-3	MPS	565 m/s
LOI Dispersion	MPS	2.6 m/s
LOI Clean Up	RCS	7.0 m/s
LLO Minimum Loiter		1 day
LLO Altitude Maintenance	RCS	10.1 m/s
LLO Extended Loiter		3 day
Detach Orion		
LLO Altitude Maintenance	RCS	30 kg/day
DOI	RCS	19.4 m/s
PDI Settling Burn	RCS	2.2 m/s
Breaking Burn	MPS	1,798.9 m/s
Guidance Phase	MPS	216.9 m/s
PDI Dispersion	MPS	53 m/s
Approach Redesignation	MPS	3 m/s
Descent RCS	RCS	11 m/s

Table 3 Altair Descent Module Payloads

Payload	Mass (kg)
Orion	20,185[24]
Ascent Module	6,610
Airlock	1,287
Payload	500
Astronauts	328

3. Structures

The structure is the one subsystem which was calibrated, rather than estimated, using the subsystem model. Historical data of space transportation systems would suggest that the structure comprise 30% of the total vehicle mass. However, LDAC-3 specifies a structure percentage of 42% for the Altair DM. This value was provided as a model input in order to size the structure and the remaining vehicle subsystem masses appropriately. Otherwise, using the 30% value based on historical data would drastically undersize the vehicle.

Table 4 Calculated high-level dry mass breakdown for the Altair DM using DYREQT

Subsystem		Dry Mass	MGA & MR	Subtotal
Avionics	kg	257.7	103.1	360.8
Structures	kg	2,696.9	1,078.8	3,775.6
Power	kg	440.9	176.4	617.3
Engines	kg	314.4	125.7	440.1
Tanks	kg	1,953.9	781.6	2,735.5
Thermal	kg	757.3	302.9	1,060.3
Total	kg	6,421.2	2,568.5	8,989.6

4. Engines

The engine is modeled using characteristics of the RL-10. This corresponds to a thrust of 83.0 kN, an I_{sp} of 448.6 sec[27], and an oxidizer-to-fuel ratio (OFR) of 6.0. The RCS was modeled using four sets of four 100 N NTO/MMH thrusters with an I_{sp} of 300 sec[27] and an OFR of 1.75.

5. Tanks

The MPS tank configuration consists of 4 LOX tanks and 4 LH_2 tanks with L/D ratios of 2.0 and 3.5, respectively[26]. The tanks contain 5% ullage and are pressurized with gaseous helium – LOX tanks are pressurized to 40 psia, LH_2 tanks are pressurized to 30 psia. RCS tanks are spherical and pressurized to 250 psia – two fuel (MMH) and oxidizer (NTO) tanks are assumed. All tanks are composed of Al 2195 and are sized using a safety factor of 1.5.

A novel concept used by Altair is the storage of fuel cell reactants in the MPS tanks. The tanks are sized to hold the propellant required for ΔV maneuvers, plus 1% for trapped propellant, plus an additional 3% as reactants for fuel cell operation[25]. It is assumed that settling of liquid propellants is accomplished via propellant settling maneuvers that are performed by the RCS. LADs are traditionally incorporated to ensure the delivery of liquid propellant to the engine and avoid ingestion of foam and or/bubbles that can often form within the tank during operations. The maneuver settles and positions the MPS propellant, removing the need for a LAD, and thus avoiding the additional 53.7% in mass per MPS tank.

6. Thermal Control

It is assumed that thermal managment of the cryogenic propellants occurs via passive methods alone. LOX and LH_2 tanks utilize 30 layers of MLI, each with 6, 9, and 15 layers in the inner, middle, and outer segments, respectively, and corresponding densities of 8, 12, and 16 layers/cm. In addition, each tank utilizes SOFI with a thickness of 25 mm[28] and a density of 36.8 kg/m^3. Boil-off is determined by the thermodynamic properties of the cryogenic fluid, the thermal environment, and the duration for which the fluid is stored. The storage duration is assumed to begin with the start of the mission (i.e. launch) and end once the DM lands on the lunar surface – a total duration of eight days. While a non-negligible amount of LOX and LH_2 remain in the tank after touchdown, the fuel cells require gaseous oxygen and hydrogen to operate. Thus, it is assumed that boil-off occurring during this phase of the mission is not as much of a concern when compared with the in-space portion of the mission. Regarding the thermal environment, Altair spends its time in in-space and on the lunar surface, with the latter being the most constraining thermal environment of the two[26]. Thus, the thermal environment corresponding to the lunar surface was used when modeling the thermal control subsystem. The following values for lunar surface properties were used: a surface temperature 207 K , a surface albedo of 0.12[25], and a beta angle of zero[25, 26] (the angle between the solar vector and the local zenith vector, with the minimum occurring at local noon[17]).

C. Validation Results

The sizing results obtained for the Altair DM using DYREQT and the suite of lunar lander subsystem models are presented in Table 4. Table 5 provides a more detailed mass breakdown; the table lists the Altair DM masses alongside

the masses obtained from the M&S enviroment. It is useful here to note that the table is representative of the level of detail that was available regarding the DM. For example, as can be seen in Table 5, the Avionics subsystem is comprised of three components – C&DH, C&T, and GN&C – each with corresponding masses, while other subsystems such as Structures, Power, Propulsion, and Thermal Control have no additional detail regarding their components and only have a subsystem mass available. Also listed are the masses for non-propellant fluids, the total propellant required for all ΔV maneuvers, and equipment for extravehicular activities (EVAs).

Masses that are predicted reasonably well include the Avionics and Structures subsystems, and Non-Prop Fluids. The ability of the model to predict the structure mass with a fairly high degree of accuracy is expected since the subsystem was calibrated for Altair (Section III.C). The Avionics mass scales, in part, with the vehicle mass, and thus benefits from the accuracy of the structure mass. The Non-Prop Fluids category consists of fuel cell reactants and miscellaneous fluids. Polsgrove allots an additional 3% of the MPS propellant for fuel cell reactants. Based on this percentage, 932.8 kg was obtained for the mass of the fuel cell reactants with the remaining 278.2 kg allotted to miscellaneous fluids.

Masses that are overpredicted include Propellant, Propulsion, Thermal Control, and Power. One possible cause for the increase in propellant mass may be due to the additional propellant carried in order to compensate for boil-off losses incurred over the course of the nine day transit from LEO to the lunar surface; neither Polsgrove, Stephan, nor LDAC-3 include any such discussion with respect to boil-off. The rates obtained from the Thermal Control subsystem model were a conservative 1.4 %/day and 0.2 %/day for LH_2 and LOX, respectively. It is also possible that a slightly different mission was modeled compared to the mission that produced the mass breakdown in Table 5. The mass overage in the Propulsion and Thermal Control categories can be attributed to the cascading effect caused by the additional propellant – an increase in the propellant mass leads to an increase in the tank size and thus tank mass, insulation mass, and the mass of associated components as they are dependent on the dimensions of the propellant tank. Regarding the difference in the mass of the Power subsystem, the model is based on heritage fuel cell technology used on the Shuttle. It is quite possible that Altair is assuming more advanced technologies.

The M&S environment calculated a vehicle dry mass of 6,421 kg and a total vehicle mass of 34,944.2 kg for the Altair DM. After applying a 20% margin each for Mass Growth Allowance (MGA) and Manager's Reserve (MGR), the total vehicle mass came to 37,513 kg. These values correspond to a difference of +3.5% and +7.8% in the dry mass and total vehicle mass of the Altair DM, respectively. Given the level of detail included in the subsystem models, and the ability to size and subsequently analyze the effects at the architecture level in a fairly short amount of time, the error is considered reasonable. These results increase confidence in the predictive capability of the suite of lunar lander modules developed. Note that optimization was not used to size the DM as the mission and vehicle inputs were known – the M&S environment only needed to size vehicle. An example that employs optimization in the sizing scheme is provided in the next section.

V. Example: Reusable Cargo Lunar Lander

This M&S environment was used to explore lunar landers that could potentially be used to support the goal of returning to the Moon [29]. This section presents the use of this environment to demonstrate the analysis of an uncrewed, cargo lunar lander. This concept is a reusable cargo lander that utilizes in-space refueling at Gateway in lunar near rectilinear halo orbit (NRHO). The lander has two design missions: an initial deployment to the moon to deliver cargo and return to NRHO, and a reuse cycle that will land payload on the lunar surface after having refueled at Gateway. This CONOPS is shown in Figure 3.

A. Lunar Lander Sizing Missions

The initial deployment phase of the mission captures the ability to directly land cargo – the deployment payload – to the lunar surface. By sending the lander straight to the moon, the first payload is delivered independent of subsequent mission events. In this mission phase, the lander is responsible for all propulsive maneuvers after TLI – LOI, insertion into LLO, and the descent to the lunar surface. Once on the surface, the lander unloads the cargo over the course of a 12 day surface stay. Once payload delivery and surface stay have commenced, the lander ascends from the surface, performs the necessary orbital transfers to LLO and NRHO, and docks with Gateway. The ΔV budget for the deployment mission and other key mission events that were used to size the reusable lander can be seen in Table 6.

The *reuse cycle* phase of the mission begins after the lander has arrived at Gateway. An new payload – the reuse payload – is loaded on to the lander, and the propellants are refueled. The mission then involves the necessary propulsive maneuvers to navigate from Gateway to the lunar surface. Similar to the deployment phase, the lander unloads the payload, loiters for 12 days of the surface, and then performs the necessary propulsive maneuvers to return to Gateway.

Table 5 Mass breakdown of the Altair DM vs. the masses obtained using DYREQT

Category	Sub-Category	Values (kg)	
		Altair[27]	DYREQT
Avionics	C&DH	202.7	–
	C&T	10.8	–
	GN&C	48.4	–
	Subtotal	261.8	262.2
Structures	**Subtotal**	2,655.7	2,856.5
Non-Prop Fluids	Fuel Cell Reactants	–	932.8
	Other	–	278.2
	Subtotal	1,211.0	1,211.0
Power	Fuel Cells	273.9	440.9
Propellant	for ΔV	24,890.1	26,616.9
Propulsion	Tanks	–	1,825.4
	Engines	–	314.4
	Subtotal	2,513.2	2,995.6
Thermal	CFM	–	515.7
	Radiator	–	259.0
	Subtotal	499.4	1,101.8
EVA	Equipment	5.1	–
Vehicle	Dry Mass	6,204.0	6,801.2
	Inert Mass	7,420.0	7,632.2
	Subtotal	32,310.1	34,944.2
	MGA	20%	20%
	MR	20%	20%
	Total	34,791.0	37,513.48

The arrival of the lander at Gateway marks the end of a single reuse cycle, and another begins with the departure of the fully fueled lander. This reuse cycle can be repeated through the expected lifetime of the lander. The ΔV budget for the deployment mission and other key mission events that were used to size the reusable lander can be seen in Table 7.

Equations for the lunar descent and ascent ΔV, Equations 26a and 26b, are listed as part of the ΔV budgets in both Tables 6 and 7. These ΔV curves were regressed based on data derived from Altair design studies.[23, 29] Both curves are based on the thrust-to-Earth-weight ratio at the beginning of either the descent or ascent phase. Additionally, the ascent phase curve is a function of the vehicle's I_{sp} to account for propulsion system-based differences in gravity losses.

$$\Delta V_{descent} = 1911.67 + 1.92 \left[\frac{F}{W_0} \right]^{-2.82} \tag{26a}$$

$$\Delta V_{ascent} = 1698.87 + 0.10 I_{sp} + 1.33 \left[\frac{F}{W_0} \right]^{-3.33} \tag{26b}$$

In practice, both of these sizing missions were combined into a single CONOPS within DYREQT. This enables three

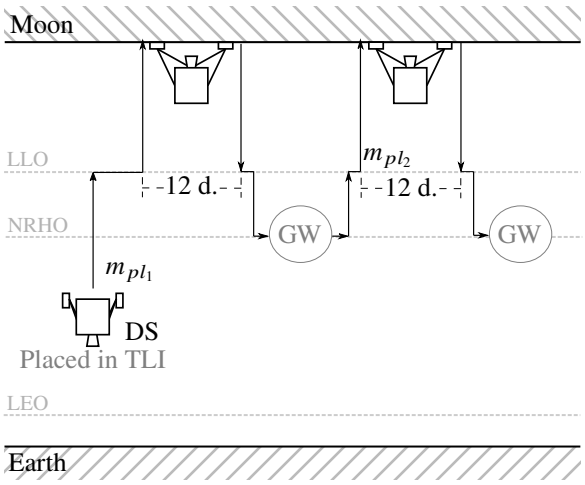

Fig. 3 Lander CONOPS

things. First it enforces the same vehicle for both the deployment and the reuse mission without needing an external loop to force convergence. Second, this allows for the two different payloads to be weighted differently in the optimization of the vehicle– a solution that prioritizes deployment payload is different from a solution that prioritizes reuse payload. Finally, it enables the simulation of launching a partially-fueled lander for the deployment mission if the lander's tanks are sized to the reuse mission.

B. Lunar Lander Vehicle

The lander is equipped with a single pump-fed LOX/LH_2 engine with an I_{sp} of 450 seconds. This engine is fed by a total of four (two oxidizer and two fuel) tanks composed of AL 2195. Helium is used as a pressurant. The tanks module described in Section III.E calculates the dimensions and weight of the propellant tanks. The total diameter of the lander is driven by the calculated diameter of the propellant tanks; this total diameter is calculated by Equation 27.

$$d_{lander} = 2 \times 1.2 \max(d_{fuel}, d_{ox}) \tag{27}$$

The RCS consists of four sets of four pressure-fed, 100 lbf NTO/MMH thrusters with an I_{sp} of 300 seconds. The vehicle has two pairs of propellant tanks which are pressurized at 4500 psi with additional helium to pressurize the system as RCS fuel is used.

The MPS is supported by an RBO CFM system. The fuel tanks share a single dedicated cryocooler, and BAC shields incorporated in each tank; oxidizer tanks utilize the same configuration. Each propellant tank is covered in 30 layers of MLI and SOFI with a density of 36.8 kg/m^3 and a thickness of 25 mm.

The power generation capability of the lander is accomplished through the use of photovoltaic cells. The cells are sized to power all of the spacecraft's subsystems and charge supplemental batteries carried aboard. The battery system consists of rechareable lithium ion batteries and is sized to power spacecraft subsystems during a one-hour LLO eclipse; during this time the CFM system is assumed to be throttled down and does not require its full energy output.

In addition to the underlying assumptions for these subsystems, it is assumed that 30% of the basic mass is allocated for structures. This percentage is higher than the average spacecraft structural percentage presented in Section III.C; this is to account for the additional mass of the landing gear. Finally, a 25% MGA is placed on the computed basic mass, and a 2.5% flight performance reserve (FPR) is allocated for all propulsive maneuvers.

1. MDAO Problem

The sizing analysis utilized the non-linear Gauss Seidel to converge the six contributing (subystem) analyses as well as the SciPy's sequential least-squares quadratic programming (SLSQP) optimizer to optimize the system and meet constraints. The SLSQP optimizer is given five degrees of freedom: the thrust of the MPS, deployment payload, reuse payload, and the L/D ratio of the fuel and oxidizer tanks. The MDAO problem is constrained such that the lander fits on the larger launch vehicle described in NASA's NextSTEP solicitation; this launch vehicle has a TLI capability of 16,000

Table 6 Deployment Mission

	Event	Propulsion System	Metric
Deployment Phase	TCM 1	RCS	20 m/s
	Lunar Transit		2 days
	Mid-course TCM 2	RCS	5 m/s
	Lunar Transit		2.1 days
	TCM 3	RCS	5 m/s
	LOI	MPS	880 m/s
	LLO TCM	RCS	10 m/s
	Loiter		0.5 d
	Descent RCS 1	RCS	15 m/s
	Lunar Descent	MPS	Eqn. 26a
	Descent RCS 2	RCS	10 m/s
	Terminal Descent	MPS	50 m/s
	Detach Deploy. P/L		$-\Delta m$ kg
	Surface Stay		12 days
	Ascent RCS 1	RCS	10 m/s
	Ascent	MPS	Eqn. 26b
	Ascent RCS 2	RCS	5 m/s
	NRHO Transfer	MPS	646 m/s
	TCM 4	RCS	10 m/s
	NRHO Transfer		0.5 days
	NRHO Insertion	MPS	84 m/s
	Docking RCS	RCS	5 m/s
	Dock at Gateway		

kg and a dynamic envelope of 6.35 m. [30]

Normally, the objective function of a vehicle MDAO problem would be to either maximize payload mass or minimize weight, but the multi-mission aspect of this problem necessitates a different objective function. The goal of this sizing analysis was to prioritize the payload delivered by the deployment mission– the more difficult of the two missions in terms of ΔV. Conversely, if the reuse payload was prioritized, the optimizer would find a solution where the deployment mission carries little to no payload. The final objective used for this analysis maximized an overall evaluation criterion that consists of the deployment payload added to the reuse payload multiplied by 0.1; this function ensures that the deployment payload is prioritized while incentivizing the optimizer to utilize the vehicle's capability for its reuse cycle. The specific objective function given to the SLSQP optimizer can be seen in Equation 28, where the optimizer maximizes the fraction of the vehicle gross mass divided by the overall evaluation criterion for payload.

$$minimize\Big(\frac{m_{gross}}{p_{deployment} + 0.1 p_{reuse}}\Big) \tag{28}$$

2. Results for the Reusable Cargo Lunar Lander

The resulting high-level mass breakdown for the reusable cargo lunar lander vehicle obtained using DYREQT is presented in Table 8. As sized, the lander launches partially fueled in order to meet the 16,000 kg TLI mass constraint. The deployment payload is determined to be 1,120 kg, and the reuse mission payload is 1,732 kg. The tanks of the lander are sized to accommodate the slightly larger propellant mass of the reuse mission. In addition to the calculated masses, the SLSQP optimizer determined that the MPS produce 11,171 lbs (49.7 kN) of thrust. The optimizer shaped

Table 7 Reuse Cycle

Reuse Cycle	Attach Reuse P/L		$+\Delta m$ kg
	Top-off Propellants	MPS&RCS	
	Undock from Gateway		
	LLO Transfer Burn	MPS	84 m/s
	TCM 1 to LLO	RCS	10 m/s
	Transfer Duration		0.5 days
	LOI Burn	MPS	646 m/s
	LLO TCM	RCS	20 m/s
	Descent RCS 1	RCS	15 m/s
	Lunar Descent	MPS	Eqn. 26a
	Descent RCS 2	RCS	10 m/s
	Vertical Drop	MPS	50 m/s
	Surface Stay		12 days
	Detach Reuse P/L		$-\Delta m$ kg
	Takeoff	MPS	50 m/s
	Ascent RCS 1	RCS	10 m/s
	Ascent	MPS	Eqn. 26b
	Ascent RCS 2	RCS	5 m/s
	NRHO Transfer	MPS	646 m/s
	NRHO Transfer TCM	RCS	10 m/s
	NRHO Insertion	MPS	84 m/s
	Docking RCS	RCS	5 m/s
	Dock at Gateway		

the propellant tanks such that the oxygen tanks were spherical while the hydrogen tanks were cylindrical in order to meet the 6.3 m dynamic envelop constraint. Finally, the RBO CFM system limits the boil-off of the hydrogen propellant to 1.3 kg/day.

This result shows the capability of the lunar lander MDAO environment within DYREQT. The SLSQP optimizer performed a multi-mission vehicle optimization with multiple contributing analyses and two dynamic equations for ΔV. Furthermore, this result shows the feasibility of a reusable cargo lunar lander; this concept could be used in the future to sustain a lunar base.

VI. Conclusion

The M&S environment presented in this paper enables lunar lander trade studies through the use of a detailed MDAO environment. This represents an advance over commonly used spreadsheet models. While the environment presented here is specialized for lunar landers, similar specializations can be made for other space transportation systems. Additionally, as was demonstrated through the integration of CryoSIM, the fidelity level of the MDAO environment can be improved through the integration of existing engineering codes.

This environment enabled a related study which investigated how a robotic mid-sized reusable lunar lander can be extended to play a larger role in Artemis, a crewed lunar exploration program.[29] This study ran over 560,000 individual lander designs in order to explore this multi-modal tradespace and would have been impossible without the capabilities of this environment.

Finally, this validation serves as a key result as it validates the sizing algorithms within the DYREQT framework when used in conjunction with a library of subelements (or subsystems). This capability will continue to be enhanced through the further development of subelements; this will improve the fidelity of existing modules and allow for

Table 8 Reusable Lunar Lander Mass Breakdown

Category	**Mass (kg)**
Avionics	217
Structures	909
Power	390
Tanks	647
Engines	213
Thermal Control	652
Total Dry	3030
MGA	757
Inert Mass	3788
Deployment Mission	
MPS Propellant	10733
RCS Propellant	358
Wet Mass	14879
Payload Mass	1120
Gross Mass	16000
Reuse Mission	
MPS Propellant	10774
RCS Propellant	307
Wet Mass	14869
Payload Mass	1732
Gross Mass	16601

additional contributing analyses to be added to the framework.

VII. Acknowledgments

This work was supported by NASA Marshall Spaceflight Center under the Engineering Services and Sciences Capability Augmentation contract partnered with Jacobs Engineering. We would like to thank Stephen Edwards and Doug Trent for their work on DYREQT and for their input into this work. We would also like to thank D.R. Komar at NASA Langley Research Center for providing insight into spacecraft power systems.

References

[1] "Artemis Plan: NASA's Lunar Exploration Program Overview," Tech. Rep. NP-2020-05-2853-HQ, National Aeronautics and Space Administration, September 2020.

[2] Edwards, Stephen J., Diaz, M. J., Mavris, D. N., and Trent, D., "A Model-Based Framework for Synthesis of Space Transportation Architectures," *2018 AIAA SPACE and Astronautics Forum and Exposition*, American Institute of Aeronautics and Astronautics, 2018. https://doi.org/10.2514/6.2018-5133.

[3] Trent, Douglas, and Mavris, D. N., "Impacts on High-level Systems-of-Systems Figures of Merit due to Integrated Architecture Sizing and Technology Evaluation at the Subsystem-Level," *2018 AIAA SPACE and Astronautics Forum and Exposition*, American Institute of Aeronautics and Astronautics, 2018. https://doi.org/10.2514/6.2018-5408.

[4] Trent, Douglas J., "Integrated Architecture Analysis and Technology Evaluation for System of Systems Modeled at the Subsystem Level," Ph.D. thesis, Georgia Institute of Technology, 2017.

[5] Olds, John R., "A Review of Technology Assessment Methods for Space Transportation Systems," *Georgia Tech Space Systems Engineering Conference*, 2005.

[6] Komar, David, Hoffman, J., Olds, A., and Seal, M., "Framework for the Parametric System Modeling of Space Exploration Architectures," *AIAA SPACE 2008 Conference & Exposition*, American Institute of Aeronautics and Astronautics, 2008. https://doi.org/10.2514/6.2008-7845.

[7] Gray, Justin, Moore, K., Hearn, T., and Naylor, B., "A Standard Platform for Testing and Comparison of MDAO Architectures," *53rd AIAA/ASME/ASCE/AHS/ASC Structures, Structural Dynamics and Materials Conference*, American Institute of Aeronautics and Astronautics, 2012. https://doi.org/10.2514/6.2012-1586.

[8] Gray, Justin S., Hwang, J. T., Martins, J. R. R. A., Moore, K. T., and Naylor, B. A., "OpenMDAO: An open-source framework for multidisciplinary design, analysis, and optimization," *Structural and Multidisciplinary Optimization*, Vol. 59, No. 4, 2019, pp. 1075–1104. https://doi.org/10.1007/s00158-019-02211-z.

[9] Wertz , Everett J., and Pushcell, J., *Space Mission Engineering: The New SMAD*, Microcosm Press, 2011.

[10] Arney, Dale C., Jones, C. A., Klovstad, J. J., Komar, D. R., Earle, K., Moses, R., and Shyface, H. R., "Sustaining Human Presence on Mars Using ISRU and a Reusable Lander," *AIAA SPACE*, 2015. https://doi.org/10.2514/6.2015-4479.

[11] "Artemis Results of the Engineering Feasibility Study," Tech. rep., NASA Johnson Space Center, 1991.

[12] Oleson, Steven R., "Concurrent Multidisciplinary Preliminary Assessment of Space Systems (COMPASS) Final Report: Advanced Long-Life Lander Investigating the Venus Environment (ALIVE)," Tech. rep., Glenn Research Center, 2018.

[13] Heineman, Willie, and Teixeira, C., "Design Mass Properties II: Mass Estimating and Forecasting for Aerospace Vehicles Based on Historical Data," Tech. rep., National Aeronautics and Space Administration, 1994.

[14] Polsgrove, Tara, Thomas, D., Sutherlin, S., Stephens, W., and Rucker, M., "Mars Ascent Vehicle Design for Human Exploration," *AIAA SPACE*, 2015. https://doi.org/10.2514/6.2015-4416.

[15] Wertz, James R., and Larson, W. J., *Space Mission Analysis and Design*, McGraw-Hill, 2010.

[16] Humble, Ronald W., Larson, W. J., and Henry, G. N., *Space Propulsion Analysis and Design*, McGraw-Hill, 1995.

[17] Sutherlin, Steven, and Johnson, W., *Cryogen Storage Integrated Model (CryoSIM) Version 3*, NASA Marshall Space Flight Center, Oct. 2014.

[18] Chapman, J. M., "Intro to Rocket Science: Sizing an In-Space Pressure Regulated Hypergolic Propulsion System," , 2016.

[19] Hastings, L. J., Hedayat, A., and Brown, T. M., "Analytical Modeling and Test Correlation of Variable Density Multilayer Insulation for Cryogenic Storage," Tech. rep., NASA Marshall Space Flight Center, 2004.

[20] Plachta, D. W., Johnson, W. L., and Feller, J. R., "Cryogenic Boil-Off Reduction System Testing," *50th AIAA/ASME/SAE/ASEE Joint Propulsion Conference*, 2014.

[21] Plachta, David W., Christie, R. J., Carlberg, E., and Feller, J. R., "Cryogenic propellant boil-off reduction system," *AIP Conference Proceedings*, Vol. 985, AIP, 2008, pp. 1457–1466.

[22] Larson, Wiley J., and Pranke, L. K., *Human Spaceflight Mission Analysis and Design*, 2007.

[23] Kos, Larry, Polsgrove, T., Sostaric, R., Braden, E., Sullivan, J., and Le, T., "Altair Descent and Ascent Reference Trajectory Design and Initial Dispersion Analyses," *AIAA Guidance, Navigation, and Control Conference*, American Institute of Aeronautics and Astronautics, 2010. https://doi.org/10.2514/6.2010-7720.

[24] National Aeronautics and Space Administration, "Lunar Capability Concept Review (LCCRR)," , Jun. 2008. Report to the PSS.

[25] Polsgrove, Tara, Button, R., and Linne, D., "Altair Lunar Lander Consumables Management," *AIAA SPACE 2009 Conference & Exposition*, 2009.

[26] Stephan, Ryan A., "Overview of the Altair Lunar Lander Thermal Control System Design and the Impacts of Global Access," *41st International Conference on Environmental Systems*, 2011.

[27] National Aeronautics and Space Administration, "LDAC-3 Mass Position - SORTIE," , 2008. Presentation.

[28] Fesmire, J. E., Coffman, B. E., Meneghelli, B. J., and Heckle, K. W., "Spray-on foam insulations for launch vehicle cryogenic tanks," *Cryogenics*, Vol. 52, No. 4-6, 2012, pp. 251–261. https://doi.org/10.1016/j.cryogenics.2012.01.018.

[29] Robertson, Bradford E., Mendez-Ramos, E., and Mavris, D. N., "A Conceptual Design Study for an Unmanned, Reusable Cargo Lunar Lander," *70th International Astronautical Congress 2019*, 2019.

[30] National Aeronautics and Space Administration, "Next Space Technologies for Exploration Partnerships - 2 Appendix E: Human Landing System Studies, Risk Reduction, Development, and Demonstration Broad Agency Announcement NNH19ZCQ001K Appendix E," , Feb. 2019.